1-1-2001

Intramolecular (Electron) Delocalization Between Aromatic Donors and their Tethered Cation–Radicals. Application of Electrochemical and Structural Probes

Duoli Sun
University of Houston

Sergey V. Lindeman
Marquette University, sergey.lindeman@marquette.edu

Rajendra Rathore
Marquette University

Jay K. Kochi
University of Houston

Accepted version. *Journal of the Chemical Society, Perkin Transactions 2,* No. 9 (2001): 1585-1594. DOI.
Sergey V. Lindeman was affiliated with the University of Houston at the time of publication.

Intramolecular (electron) delocalization between aromatic donors and their tethered cation–radicals. Application of electrochemical and structural probes

Duoli Sun
Department of Chemistry, University of Houston, Houston, TX
Sergey V. Lindeman
Department of Chemistry, University of Houston, Houston, TX
Rajendra Rathore
Department of Chemistry, University of Houston, Houston, TX
Jay K. Kochi
Department of Chemistry, University of Houston, Houston, TX

Abstract

To study the mechanism of electronic transduction along (poly)phenylene chains, a series of aromatic donors with general formula **D**–**B**–**D** has been synthesized [where **D** = 2,5-dimethoxy-4-methylphenyl donor and **B** = (poly)phenylene bridge]; and the corresponding cation–radical salts **D**–**B**–**D**$^{+\cdot}$ $SbCl_6^-$ have been isolated for X-ray crystallographic analyses. The magnitude of the electronic interaction between the **D** and **D**$^{+\cdot}$ moieties through the various **B** bridges has been measured (i) as the difference between the first and the second oxidation potentials of **D**–**B**–**D** donors and (ii) as the structural changes induced in neutral **D** by the presence of the tethered **D**$^{+\cdot}$ group in **D**–**B**–**D**$^{+\cdot}$ cation–radicals. The intramolecular interaction of **D** and **D**$^{+\cdot}$ groups was found to occur via π-conjugation of the bridging (poly)phenylene group. As such, the electronic interaction is highly dependent on the planarity of the (poly)phenylene bridge, and can be either inhibited or promoted by the deliberate modifications of the molecular conformation. Crystal structures of compounds **A**, **B**, **B**$^{+\cdot+\cdot}$, **1**, **1**$^{+\cdot}$, **2**, **2**$^{+\cdot}$, **3**$^{+\cdot}$, **8** and **9**$^{+\cdot}$ are reported.

Introduction

Structural and electronic aspects of long-range chemical transduction are important to modern supramolecular chemistry; and chemical systems of the general structure: **D**^{1}–**B**–**D**^{2} are considered to be prototypes of nanoscale electronic devices such as chemical sensors, switches, wires etc.[1–3] In these molecular systems, the application of some physical/chemical action to the primary group **D**^{1} (e.g. irradiation, complexation, protonation, reduction/oxidation) induces changes in its structure/electronic state. The effect of these changes is subsequently transmitted through the [extended] bridging group **B** to the [remote] **D**^{2} moiety. The structural/electronic/optical reply of the **D**^{2} moiety can then produce either a desirable target effect or begin another chain of physical/chemical transformations.

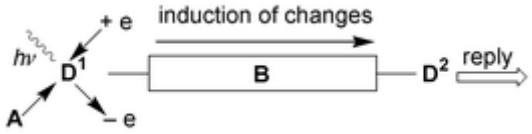

In this study, we examine the structural and electronic reply of a remote donor group **D**^{2} upon the removal of one electron from the primary donor group **D**^{1} that is separated from **D**^{2} through different bridging (poly)-p-phenylene moieties **B**. As such, we initially focus on the simple symmetrical system: **D**–**B**–**D**, where **D** is the 2,5-dimethoxy-4-methylphenyl donor group.

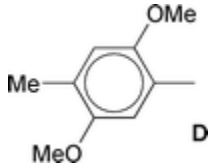

D is a good electron donor (E_{ox}^0 = 1.1 V vs. SCE) that allows its ready oxidation electrochemically and by a variety of chemical oxidants.[4] The resulting cation–radicals are relatively persistent and can be reversibly reduced back to the original neutral donors. Importantly, p-dimethoxy-substituted aromatic groups exhibit relatively large geometrical changes during oxidation, and this makes them desirable structural indicators—even for small amounts (<0.1 e) of charge redistribution. Importantly, these

groups do not show significant intermolecular self-association upon oxidation as opposed to the majority of other aromatic electron donors (naphthalene, anthracene etc.).[5]

$$D + D^{+\bullet} \rightleftharpoons (D_2)^{+\bullet}$$

Consequently, the intramolecular effects can be readily differentiated from those derived from intermolecular interactions.

The three classes of aromatic donors examined in this study are represented in Chart 1. The Class I donors contain two **D** groups linked through a (poly)phenylene chain of different length. Class II includes donors in which the rotation about the bridging phenylene moiety is restricted by the presence of one or more methyl groups. Class III donors contain a modified (either planarized or an extended) (bis)phenylene bridging group. We approach this problem by simultaneously applying electrochemical (cyclic voltammetry and Osteryoung square-wave voltammetry)[6] as well as structural (X-ray crystallography) techniques to probe the electronic interaction of **D** and $\mathbf{D}^{+\bullet}$ through the agency of various types of polyphenylene bridges.

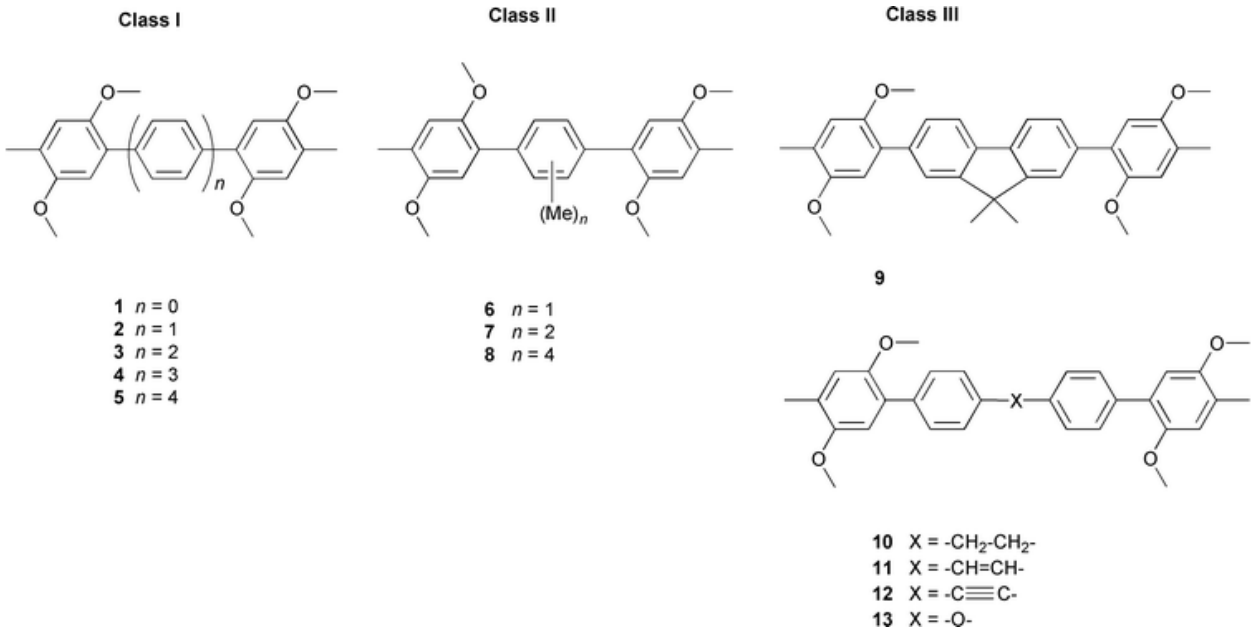

1 $n = 0$
2 $n = 1$
3 $n = 2$
4 $n = 3$
5 $n = 4$

6 $n = 1$
7 $n = 2$
8 $n = 4$

9

10 X = -CH_2-CH_2-
11 X = -CH=CH-
12 X = -C≡C-
13 X = -O-

Chart 1

Results and discussion

I. Group D as the electrochemical/structural probe

For the electronic transduction process, we first examined the structural change of the model donors **A** and **B** upon electrochemical oxidation. The cyclic voltammogram (CV) of the monobenzenoid donor **A** showed a characteristic (1-electron) reversible wave at $E_{ox}^0 = 1.10$ V vs. SCE with peak separation of $E_{pa} - E_{pc} = 60$ mV in dichloromethane solution at a scan rate of 100 mV s^{-1}.

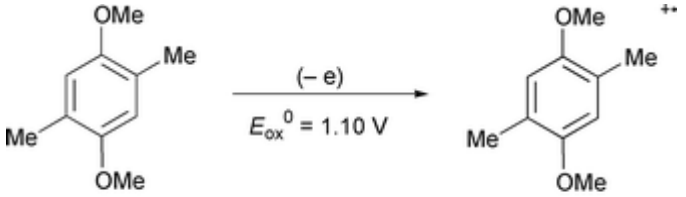

D-Me (**A**) D-Me$^{+\bullet}$ (**A**$^{+\bullet}$)

Essentially the same cyclic voltammogram was obtained with the bis-benzenoid donor **B**; but calibration of the CV wave showed that the anodic oxidation was composed of a 2-electron process. Since such a CV characteristic suggested the identical behavior of two independent **D** moieties in the donor **B**, we examined the molecular structure of the dication in the following way. The dicationic salt of the bis-benzenoid donor **B** was successfully isolated as a (black) crystalline solid with stoichiometry: **D**$(CH_2)_3$**D**$^{2+}(SbCl_6)_2^-$, as described in the Experimental section. Single crystal X-ray crystallography established the presence of a crystallographic symmetry (mirror plane) to demonstrate that both **D** moieties are identical, and both bear a unit of positive charge. Therefore, it is easy to conclude that **B**$^{++}$ is in fact the dication–diradical (**B**$^{+\bullet+\bullet}$). The pertinent aromatic C–C bond distances in **B** and **B**$^{+\bullet+\bullet}$ are listed in Table 1, together with those of the monobenzenoid donor **A**.

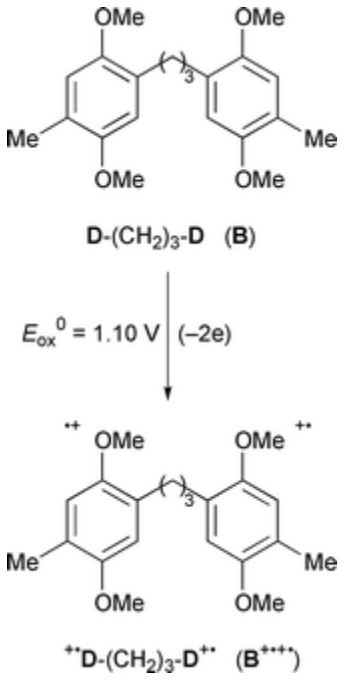

D-$(CH_2)_3$-D (**B**)

$^{+\bullet+\bullet}$D-$(CH_2)_3$-D^{++} (**B**$^{+\bullet+\bullet}$)

Table 1 Electrochemical and structural parameters of **A**, **B** and **B**$^{+\bullet+\bullet}$

	Donor	E_{ox}/V vs. SCE	Bond lengths/Å[a]					Coulombic charge q_i
			α	β	γ	δ	ε	
A	**D**–CH_3	1.10	1.401	1.394	1.396	1.380	1.426	0
B	**D**–$(CH_2)_3$–**D**	1.10	1.399	1.396	1.397	1.375	1.425	0
B$^{+\bullet+\bullet}$	$^{+\bullet}$**D**–$(CH_2)_3$–**D**$^{+\bullet}$		1.447	1.407	1.372	1.327	1.457	+1

[a] **Averaged over four and two chemically equivalent values for structures B and B**$^{+\bullet+\bullet}$**, respectively.**

Examination of the structural parameters in Table 1 showed that the neutral **D** moiety has the usual planar centrosymmetric benzenoid geometry, as can readily be seen from the pertinent aromatic bond lengths. Thus the endocyclic C–C bond lengths α, β and γ are all equal within the standard (1.397–1.400 Å) range.[7] Furthermore, the exocyclic C(Ar)–O (δ) and C(Me)–O (ε) bond lengths of 1.375(1) and 1.424(1) Å are also close to the standard values[7] of 1.370 and 1.426 Å, respectively. However, upon oxidation, the **D** moieties in $^{+\bullet}$**D**–$(CH_2)_3$–**D**$^{+\bullet}$ exhibit the significant geometric changes shown in Table 1. Although the system retains its local center of symmetry, the C–C bonds α and β are elongated by +4.7 and +1.0 pm, respectively, and the γ bonds are shortened by −2.5 pm in accord with the major contribution of the quinonoidal resonance form **Q** shown below.[8,9]

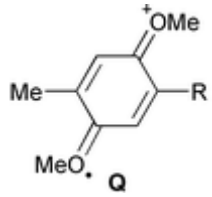

Q

Most remarkably, the exocyclic δ bonds C(Ar)–O exhibit the greatest change—being shortened by −4.8 pm. Also, the ε bonds C(Me)–O are elongated by 3.3 pm. Thus, the quinonoidal distortion of **D**$^{+\bullet}$ is a highly sensitive measure of its oxidation degree. Indeed, such large magnitudes of the geometrical changes provide confidence in our ability to distinguish between neutral and cationic oxidation states of the **D** groups, as indicated by the values of q_i in Table 1 (last column). For relatively small geometrical changes in conjugated π-systems, a simple linear regression was found to be adequate for evaluating the partial (effective) charge q_i of a particular **D** moiety, as shown in eqn. (1),[10] where q_i is the partial charge over the **D** moiety, d_0 and d_1 are values for a bond length in neutral **D** and 1-electron oxidized **D**$^{+\bullet}$, respectively (Table 1), and d_i is the pertinent bond length in the oxidized donor. For the purpose of clarity, we will hereafter focus on only the δ bonds for the calculation of q_i owing to their largest bond-length change upon oxidation.[11]

$$(1) \qquad q_i = (d_0 - d_i)/(d_0 - d_1)$$

II. Electrochemical and structural properties of Class I aromatic donors. Effects of the (poly)phenylene chain

A pair of **D** moieties linked directly together, as in donor **1**, shows two well-resolved reversible (one-electron) oxidation waves at 1.11 and 1.40 V (Table 2, Fig. 1a).[12] When the two **D** moieties are tethered through a single p-phenylene bridge (donor **2**) they also show clearly two resolved oxidation waves at 1.15 and 1.26 V (Fig. 1b). These two 1-electron waves coalesce into a single 2-electron wave at 1.18 V in donor **3** having two p-phenylene groups in the bridge (Fig. 1c). Further incorporation of p-phenylene units, as in donors **4**, **5**, does not change the simple electrochemical pattern of donor **3** (Table 2).

Table 2 Electrochemical characteristics of aromatic donors **1–13**[a] (±0.03 V)

Class	Donor	E_{ox1} [b]		E_{ox2} [b]	ΔE_{ox}
I	**1**	1.11 (1e)		1.40 (1e)	0.29
	2	1.15 (1e)		1.26 (1e)	0.11
	3		1.18 (2e)		
	4		1.18 (2e)		
	5		1.18 (2e)		
II	**6**	1.16 (1e)		1.25 (1e)	0.09
	7		1.17–1.24 (2e)		
	8		1.21 (2e)		
III	**9**	1.13 (1e)		1.19 (1e)	0.06
	10		1.17 (2e)		
	11		1.18 (2e)		
	12		1.18 (2e)		
	13		1.17 (2e)		

[a] Experimental conditions: concentration 0.5 mM in 0.1 M supporting electrolyte in dichloromethane solution at room temperature; scan rate 2 V s^{-1}; the oxidation potentials are given in V vs. SCE. b In parentheses—number of electrons transferred.

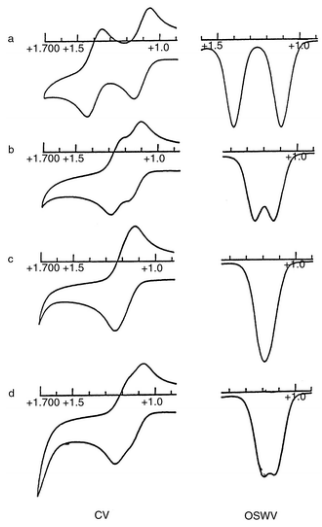

Fig. 1 Coalescence of two 1-electron oxidation waves with increasing length of p-phenylene bridge. From (a) donor **1** directly linked **D** moieties together; (b) in donor **2**, with a single p-phenylene bridge;

to (c) donor **3** with a (bis)-p-phenylene bridge. (d) The waves are split again for donor **9** with a planarized bridge.

Structurally, the D moieties in the bridged donors **1**, **2** and their cation–radicals $\mathbf{1}^{+\cdot}$, $\mathbf{2}^{+\cdot}$ and $\mathbf{3}^{+\cdot}$ (Tables 3 and 4) can be compared with the "standard" geometries (in Table 1) in the following way.

Table 3 Quinonoidal distortion and positive charge distribution between **D** moieties in $\mathbf{D–B–D}^{+\cdot}$ cation–radicals

Donor		**Group**	**δ** [a]**/Å**	**δ** [b]**/Å**	**δ** $_{av}$**/Å**	**σ** [c]	**q** $_i$ [d]
1	$\mathbf{D^1–D^2}$	$\mathbf{D^1}$, $\mathbf{D^2}$	1.373	1.379	1.376	0.002	0
$\mathbf{1}^{+\cdot}$	$[\mathbf{D^1–D^2}]^{+\cdot}$	$\mathbf{D^1}$	1.341	1.356	1.349	0.003	+0.5
		$\mathbf{D^2}$	1.344	1.356	1.350		+0.5
2	$\mathbf{D^1}$–(p-C_6H_4)–$\mathbf{D^2}$	$\mathbf{D^1}$, $\mathbf{D^2}$	1.368	1.375	1.371	0.004	0
$\mathbf{2}^{+\cdot}$	$[\mathbf{D^1}$–(p-C_6H_4)–$\mathbf{D^2}]^{+\cdot}$	$\mathbf{D^1}$	1.331	1.344	1.337	0.002	+0.8
		$\mathbf{D^2}$	1.363	1.369	1.366		+0.2
$\mathbf{3}^{+\cdot}$	$[\mathbf{D^1}$–(p-$C_6H_4)_2$–$\mathbf{D^2}]^{+\cdot}$	$\mathbf{D^1}$	1.325	1.324	1.325	0.004	+1.0
		$\mathbf{D^2}$	1.370	1.385	1.377		0.0
$\mathbf{9}^{+\cdot}$	$[\mathbf{D^1}$-(C_6H_3)-(C_6H_3)-$\mathbf{D^2}]^{+\cdot}$ 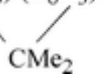	$\mathbf{D^1}$	1.351	1.365	1.358	0.003	+0.35
		$\mathbf{D^2}$	1.362	1.368	1.365		+0.2

[a] With ortho-methoxy group. b With meta-methoxy group. c Precision of structure. d Charge estimated from δ_{av} values using eqn. (1).

Table 4 Geometric parameters (Å) of the **D** moiety at different oxidation states (average values are given in parentheses)

Aromatic donor		**[σ]**[a]	**Group**	**α/α′**	**β/β′**	**γ/γ′**	**δ/δ′**	**ε /ε′**	**q** $_i$ [b]
1	D–D	0.002	D^1, D^2	1.402/ 1.394 (1.398)	1.396/ 1.399 (1.397)	1.393/ 1.393 (1.393)	1.373/ 1.379 (1.376)	1.426/ 1.424 (1.425)	0
$\mathbf{1}^{+\cdot}$	$[D–D]^{+\cdot}$	0.003	D^1	1.444/ 1.432 (1.438)	1.400/ 1.377 (1.389)	1.378/ 1.408 (1.393)	1.341/ 1.356 (1.349)	1.453/ 1.442 (1.447)	+0.5
			D^2	1.442/ 1.425 (1.433)	1.402/ 1.383 (1.393)	1.379/ 1.410 (1.395)	1.344/ 1.356 (1.350)	1.452/ 1.442 (1.447)	+0.5
2	D–(p-C_6H_4)–D	0.004	D^1, D^2	1.395/ 1.388 (1.391)	1.397/ 1.395 (1.396)	1.387/ 1.399 (1.393)	1.368/ 1.375 (1.371)	1.425/ 1.421 (1.423)	0

Aromatic donor		[σ][a]	Group	α/α′	β/β′	γ/γ′	δ/δ′	ε /ε′	q_i [b]
2 $^{+\cdot}$	[D–(p-C_6H_4)–D]$^{+\cdot}$	0.002	D^1	1.440/ 1.436 (1.438)	1.411/ 1.387 (1.399)	1.377/ 1.397 (1.387)	1.331/ 1.344 (1.337)	1.449/ 1.444 (1.447)	+0.8
			D^2	1.416/ 1.410 (1.413)	1.399/ 1.383 (1.391)	1.393/ 1.409 (1.401)	1.363/ 1.369 (1.366)	1.432/ 1.435 (1.433)	+0.2
3 $^{+\cdot}$	[D–(p-C_6H_4)$_2$–D]$^{+\cdot}$	0.004	D^1	1.446/ 1.435 (1.441)	1.411/ 1.401 (1.406)	1.371/ 1.383 (1.377)	1.325/ 1.324 (1.325)	1.454/ 1.448 (1.451)	+1.0
			D^2	1.410/ 1.396 (1.403)	1.392/ 1.392 (1.392)	1.393/ 1.410 (1.401)	1.370/ 1.385 (1.377)	1.440/ 1.419 (1.429)	0.0
9 $^{+\cdot}$	[D-(C_6H_3)-(C(CN)$_2$)–D]$^{+\cdot}$	0.003	D^1	1.431/ 1.427 (1.429)	1.399/ 1.382 (1.391)	1.382/ 1.411 (1.397)	1.351/ 1.365 (1.358)	1.437/ 1.435 (1.436)	+0.35
			D^2	1.427/ 1.413 (1.420)	1.399/ 1.388 (1.393)	1.391/ 1.415 (1.403)	1.362/ 1.368 (1.365)	1.438/ 1.431 (1.435)	+0.2

[a] **An average experimental precision. b Estimated charge/oxidation degree—from δ values and eqn. (1).**

(i) In cation–radical **1**$^{+\cdot}$, the structure of both **D** moieties is almost identical (though there is no crystallographic symmetry between them). This structure is essentially intermediate between geometries of the neutral **D** and the cationic **D**$^{+\cdot}$ group. From the evaluation of the quinonoidal distortion in Table 3 with the aid of eqn. (1), we conclude that there is equal charge (+0.5 e) on $\mathbf{D^1}$ and $\mathbf{D^2}$ in the cation–radical **1**$^{+\cdot}$.

(ii) In cation–radical **2**$^{+\cdot}$, the **D** moieties are structurally different. The geometry of $\mathbf{D^1}$ is closer to that of the cationic structure, whereas $\mathbf{D^2}$ has a more neutral geometry. However, they both differ significantly from the pure neutral and cationic geometries. From the evaluation of the quinonoidal distortion in Table 3, we conclude that there is a positive charge corresponding to the loss of 0.8 e on $\mathbf{D^1}$ and 0.2 e on $\mathbf{D^2}$ in cation–radical **2**$^{+\cdot}$.

(iii) In cation–radical **3**$^{+\cdot}$, the geometry of $\mathbf{D^1}$ reproduces the standard geometry of a cationic **D** group, whereas the $\mathbf{D^2}$ moiety does not exhibit any geometric changes relative to the neutral **D** group. From the evaluation of the quinonoidal distortion in Table 3, we conclude that $\mathbf{D^1}$ is the full cation–radical ($\mathbf{D}^{+\cdot}$), and $\mathbf{D^2}$ is equivalent to the unperturbed donor.

The magnitude of the interaction between the **D** moieties can be also quantified from electrochemical data if we take the observed splitting of the oxidation waves (ΔE_{ox}) as a qualitative indicator of the resonance energy of this interaction.[13a] As such, the resonance energy increases from 0 to 2.5 and 6.7 kcal mol^{-1} in a series **3**$^{+\cdot}$ → **2**$^{+\cdot}$ → **1**$^{+\cdot}$ and appears to be proportional to the amount of positive charge q_i transferred between **D** units (Fig. 2).[13b]

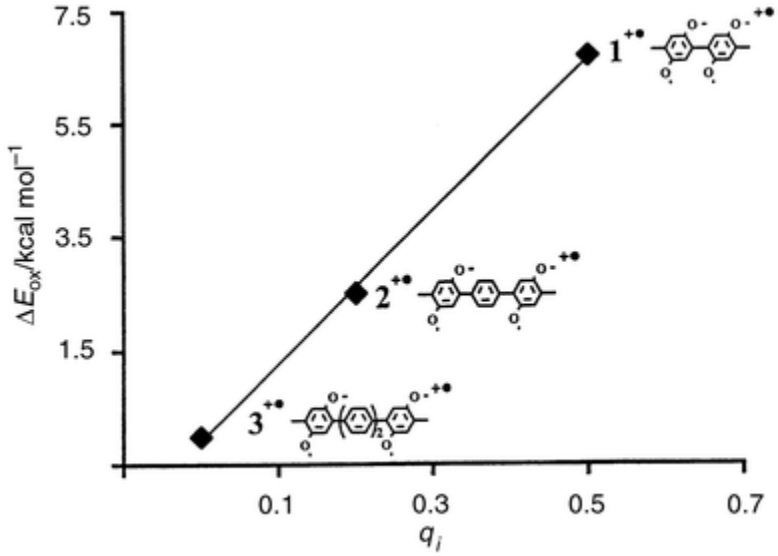

Fig. 2 Linear relationship between resonance energy ΔE_{ox} (kcal mol^{-1}) and amount of positive charge q_i distributed in the **D²** moiety in cation–radicals **1**$^{+\cdot}$, **2**$^{+\cdot}$ and **3**$^{+\cdot}$.

To better understand the mechanism of the interaction between the **D** and **D**$^{+\cdot}$ units, we examined other structural changes accompanying the oxidation of the donors **1**–**3**. Most importantly, there are some remarkable changes in the overall molecular shapes as follows.

(i) The essentially nonplanar neutral donor **1** exhibits substantial planarization as a result of its 1-electron oxidation (Fig. 3). The twist angle φ around the central C(Ar)–C(Ar) bond is reduced from 69.1 to 39.5° with an accompanying shortening of this bond from 1.491 to 1.458 Å.

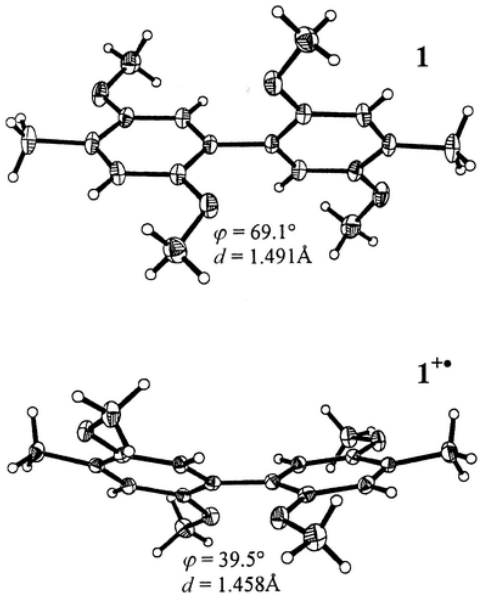

Fig. 3 Planarization of dihedral angle and contraction of bond length between **D**^{1} and **D**^{2} of donor **1** owing to 1-electron oxidation: (top) ORTEP diagram of the neutral donor **1**, (bottom) ORTEP diagram of the corresponding cation–radical **1**$^{+\cdot}$. Thermal ellipsoids are given at 50% probability level.

(ii) Donor **2** is less sterically hindered than **1** and thus less twisted around its two symmetrically equivalent C(Ar)–C(Ar) bonds by 44.9°. During 1-electron oxidation, the twist is reduced even more to φ = 32.0° and 28.6°, with a progressive shortening of the C(Ar)–C(Ar) bonds from 1.493 Å to 1.466 and 1.474 Å, respectively (Fig. 4b and c). Noticeably, the **D** group with more cationic geometry (see above) gives the shorter C–C bond with the p-phenylene bridge.

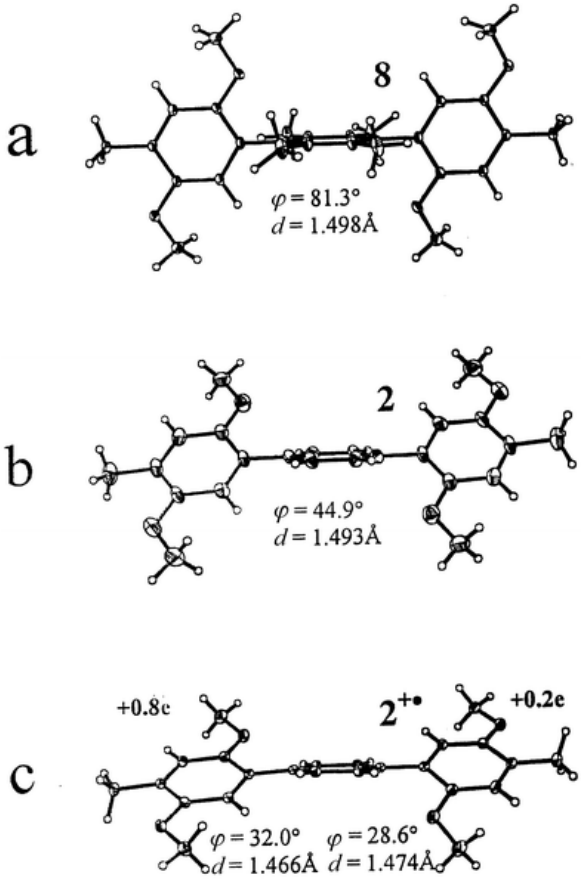

Fig. 4 Successive planarization of molecular geometry going from sterically hindered donor **8** to **2** and to its cation–radical $\mathbf{2}^{+\cdot}$. (a) ORTEP diagram of almost orthogonal donor **8**, (b) ORTEP diagram of the neutral donor **2**, (c) ORTEP diagram of planarized structure of cation–radical $\mathbf{2}^{+\cdot}$.

(iii) The cation–radical $\mathbf{3}^{+\cdot}$ has dihedral angles similar to $\mathbf{2}^{+\cdot}$ with φ = 36.4 and 31.4° between the **D** planes and p-phenylene groups. The dihedral angle between the planes of the p-phenylene rings is 16.9°. The intercyclic C(Ar)–C(Ar) bonds continuously change from 1.469 to 1.485 and to 1.488 Å on going from the positively charged to the neutral **D** moiety.

The co-planarization of aromatic π-moieties accompanied by shortening of the bonds between them indicates an increasing π–π-conjugation. A quantitative degree of the π-conjugation can be calculated through the bond orders of the corresponding C–C bonds using Pauling's theory.[14] Thus, the observed shortening of the central C(Ar)–C(Ar) bond in the molecule **1** during oxidation corresponds to changes in bond order from 1.0 to 1.15. This means that the bond becomes 30% π-conjugated in $\mathbf{1}^{+\cdot}$ (when referred to 100% conjugation in benzene). In cation–radical $\mathbf{2}^{+\cdot}$, the degree of π-conjugation between the central p-phenylene bridge and the terminal $\mathbf{D}^{+\cdot}$ and **D** groups is 20% and 10%, respectively. For

cation–radical **3**$^{+\cdot}$, conjugation does not spread further than 15% between **D**$^{+\cdot}$ and its neighboring p-phenylene group. Beyond that the π-conjugation is barely detectable.

Additional contraction of the ortho-bonds δ (as compared to meta-bonds δ′) is another indicator of π-conjugative interaction between **D**$^{+\cdot}$ and **D** moieties in **1**$^{+\cdot}$ and **2**$^{+\cdot}$ (Table 3). A detailed consideration of geometry of these groups (Table 4) shows loss of the local symmetry center and significant contribution of the ortho-quinonoidal resonance structure **Q**′.

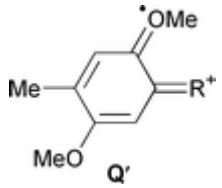

Q′

We thus conclude that interaction between **D**$^{+\cdot}$ and **D** moieties largely occurs via π-conjugation. This interaction is weakened by a bridging p-phenylene group and becomes almost undetectable when the bridge is comprised of two or more p-phenylene units.

Since π-conjugation is highly dependent structurally on geometric conditions (values of dihedral φ angles etc.), it can be both suppressed and promoted by deliberate control of the molecular conformation which affects the interaction between **D**$^{+\cdot}$ and **D**. To probe this point, we examined the Class II donors derived from the successive methylation of donor **2**.

III. Electrochemical and structural properties of Class II aromatic donors. Effects of steric hindrance

Aromatic donor **2** shows two (1-electron) oxidation waves that coalesce into one (2-electron) wave upon addition of one more p-phenylene unit in the bridge in donor **3**. The same effect can be achieved via successive methylation of the central p-phenylene bridge in Class II donors (Fig. 5, Table 2). The introduction of one methyl group shifts the pair of anodic waves together, from two oxidation potentials of 1.15/1.26 V for the parent donor **2** to 1.16/1.25 V for the monomethyl analog **6**. The presence of two methyl groups (donor **7**) makes the two waves barely distinguishable in the range 1.17–1.24 V (Fig. 5c) and these waves finally coalesce at 1.21 V for donor **8** with the permethylated p-phenylene bridge (Fig. 5d).

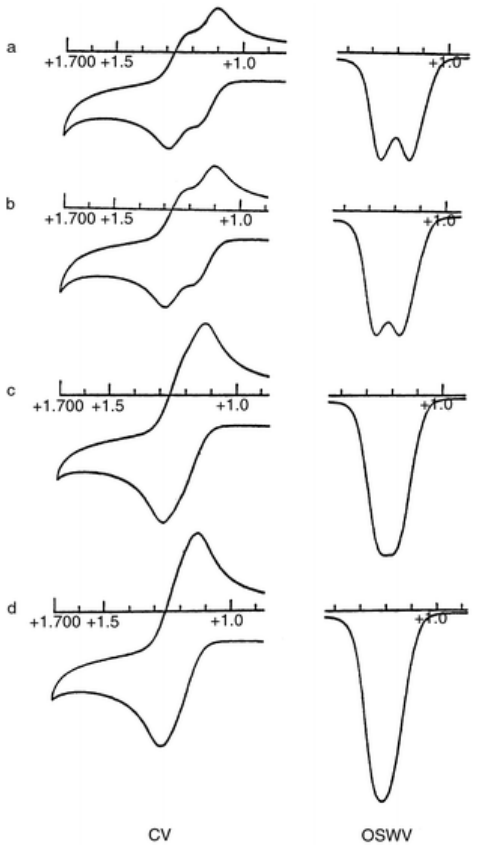

Fig. 5 Progressive coalescence of the two oxidation waves of donor **2** following mono-, di-, and tetramethyl substitution of the single p-phenylene bridge (a, b, c, and d for donors **2**, **6**, **7**, and **8** respectively).

The resonance energy of 2.5 kcal mol^{-1} in cation–radical $\mathbf{2}^{+\cdot}$ drops to 2.1 kcal mol^{-1} in cation–radical $\mathbf{6}^{+\cdot}$, 1.6 kcal mol^{-1} in $\mathbf{7}^{+\cdot}$, and to almost zero in $\mathbf{8}^{+\cdot}$. The steady fall of the resonance energy with successive methylation of the bridging p-phenylene can be attributed to increasing steric hindrance. We also see that the twist between the **D** moiety and the neighboring p-phenylene bridge is reduced during oxidation from φ = 45 to φ = 30° (Fig. 4b and 4c) in donor **2** to facilitate the increasing π-conjugation (cos φ increases from 0.71 to 0.87, respectively). The structure of donor **8** with the permethylated p-phenylene bridge reveals an almost orthogonal orientation of the groups (Fig. 4a) with φ = 81.3° that prohibits any significant π–π-interaction (cos φ = 0.15). The short intramolecular contacts between ortho-substituents (Me···OMe of 3.45 and 4.00 Å) do not allow this value to be reduced in the corresponding cation–radical $\mathbf{8}^{+\cdot}$.

Such an effect is expected from the interaction between **D** and $\mathbf{D}^{+\cdot}$ groups through a π-conjugated chain. The interaction is optimal for more or less unperturbed (coplanar) molecular conformations and fades with an increasing molecular twist. The electrochemical behavior of Class II donors strongly supports this point.

We next examined Class III donors in order to determine the role of the π-conjugation in (poly)phenylene donors, which cannot be broken but can be promoted for optimal interaction between **D** and $\mathbf{D}^{+\cdot}$ groups as described below.

IV. Electrochemical and structural properties of Class III aromatic donors. Effects of improved π-conjugation

If the existing chain of π-conjugation in cation–radical **2**$^{+\cdot}$ can be broken by the introduction of steric hindrance, can the broken chain of π-conjugation in cation–radical **3**$^{+\cdot}$ then be restored by any deliberate means?

The Class III donors represent analogs of compound **3** where the central (bis)phenylene bridge has been structurally modified to achieve a better degree of π-conjugation through it. In particular, the introduction of π-conductive groups with smaller degrees of steric hindrances at the juncture of the two p-phenylene bridging units has been considered. However, the introduction of either ethylene (**11**) or acetylene (**12**) bridges as well as an oxide bridge (**13**) did not result in any detectable conductivity of the bridge. All these compounds show the same electrochemical behavior as the parent donor **3** (and the model donor **10** with an "insulating" bis-methylene bridge), in each case a single 2-electron (reversible) oxidation wave was observed at 1.17–1.18 V vs. SCE (Table 2).

Importantly, an additional –CMe_2– link introduced between the two p-phenylene units of donor **3** afforded surprising results. For the fluorenyl-bridged compound **9** a pair of resolvable 1-electron (reversible) oxidation waves is observed at 1.13 and 1.19 V (Table 2, Fig. 1d) instead of the single (2-electron) wave at 1.18 V (Fig. 1c).

The X-ray structural study of cation–radical **9**$^{+\cdot}$ shows the geometry of both **D** moieties to be different, and intermediate between the neutral and cationic geometries (Tables 3 and 4). However, unlike cation–radical **2**$^{+\cdot}$, both **D** moieties gravitate more to the neutral than to the cationic geometry. Interestingly, the dihedral angles are not very different in cation–radical **9**$^{+\cdot}$ as compared with its parent cation–radical **3**$^{+\cdot}$. The angles between **D** groups and neighboring benzene rings are φ = 30.4 and 29.6°, and the angle between the former p-phenylene units within the bridging fluorenyl moiety is φ = 5.7° (cf.Fig. 6a and 6b). However, the intercyclic C(Ar)–C(Ar) bonds exhibit much more pronounced shortening than in **3**$^{+\cdot}$ going to 1.464 and 1.471 Å (cf. similar values of 1.466 and 1.474 Å in **2**$^{+\cdot}$). Moreover, the most affected central bond within the fluorenyl moiety is shortened to 1.433 Å. Thus, the introduction of a chemical bridge between two ortho-centers in the bridging biphenylene moiety causes dramatic changes in π-conjugation in **9**$^{+\cdot}$ as compared with the parent cation–radical **3**$^{+\cdot}$. Structural and electrochemical data suggest that cation–radical **9**$^{+\cdot}$ possesses (a) substantial resonance energy of 1.4 kcal mol^{-1} and (b) 15–20° π-conjugation between the **D** moieties and the fluorenyl bridge (the degree of π-conjugation between the former p-phenylenes can be estimated as almost 60%).

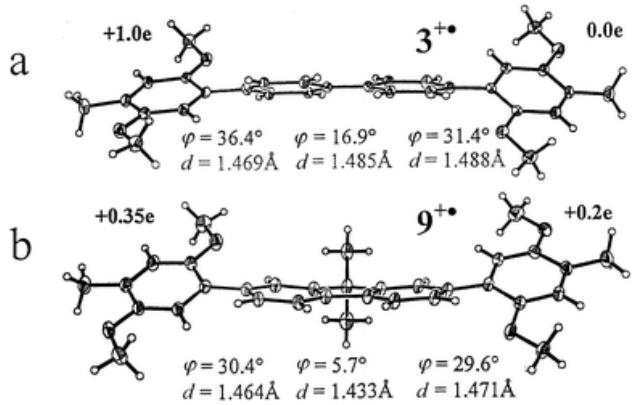

Fig. 6 Comparison of molecular geometry of (a) cation–radical **3**$^{+\cdot}$ with localized positive charge, and (b) related cation–radical **9**$^{+\cdot}$ with delocalized electronic structure.

It is important to note that the quinonoidal distortion in the cation–radical $\mathbf{9}^{+\cdot}$ (Table 3) leads to only +0.35 and +0.2 fractional positive charge on the terminal **D** groups, the remainder (+0.45 e) being associated with the fluorenyl bridge. In neither $\mathbf{2}^{+\cdot}$ nor in $\mathbf{3}^{+\cdot}$ could we detect any measurable fraction of positive charge associated with bridging p-phenylene groups. The observed charge distribution shows that in the fluorenyl moiety the p-phenylene groups lose their identity and their electron system acts jointly as a better donor than the parent p-biphenylene. We conclude that a longer (poly)phenylene chain *with the forced planarity* should possess good electric hole-conductive properties and behave as a single superdonor entity.

Summary and conclusions

Aromatic donors of general formula **D**–**B**–**D** [where **D** is a donor 2,5-dimethoxy-4-methylphenyl group and **B** is a bridging (poly)phenylene moiety] have been studied structurally and electrochemically. In the corresponding cation–radicals (**D**–**B**–$\mathbf{D}^{+\cdot}$), an electronic interaction occurs between **D** and $\mathbf{D}^{+\cdot}$ groups through the chain of π-conjugation involving the bridging group **B**.

A single bridging p-phenylene unit exhibits variable conductivity that is limited by the conformation (twist) of the molecular chain. However, the interaction between $\mathbf{D}^{+\cdot}$ and **D** groups does not propagate through two or more p-phenylene groups.

To achieve a conductivity through the bis(p-phenylene) bridge, two p-phenylene units have been brought together in a rigid co-planar fashion by a chemical $–CMe_2–$ link between their ortho-positions. The resulting fluorene-bridged derivative upon oxidation shows an (almost) uniform distribution of the positive charge along the π-conjugated molecular chain.

The positive charge distribution in **D**–**B**–**D** donors mimics electric-hole conductivity in polyphenylene sequences. The results show that the hole conductivity along polyphenylene chains is either (a) not possible (beyond the first 1 or 2 elementary units) or (b) requires a relatively high activation energy. However, the mutual co-planarization of p-phenylene units using rigid chemical links between them greatly improves their conductive properties.

We hope that UV/Vis spectroscopic and variable temperature EPR studies presently underway will provide further insight into the mechanism of such an electronic transduction.

Experimental

Materials

Methyl-p-hydroquinone, 2,5-dibromo-p-xylene, 4,4′-dibromobiphenyl, bis(triphenylphosphine)palladium(II) chloride, triethyloxonium hexachloroantimonate, and tetra-n-butylammonium hexafluorophosphate from Aldrich, Acros, or Alfa were used without further purification. 2,5-Dimethoxytoluene,[15] 4-bromo-2,5-dimethoxytoluene,[16] 4-bromobiphenyl,[17] 4-bromoterphenyl,[17] 4,4″-dibromoterphenyl,[17] 9,9-dimethylfluorene,[18] dibromodurene,[17] 2,7-dibromo-9,9-dimethylfluorene,[17] 4,4′-dibromostilbene,[19a] 4,4′-dibromotolan,[19b] 1,3-bis(2,5-dimethoxy-4-methylphenyl)propane[19c]B, and 2,5-dimethyl-1,4-dimethoxybenzene[19d]A as well as the 2,3,8,9-tetrahydro-1,1,4,4,7,7,10,10-octamethyltetracene radical–cation ($OMN^{+\cdot}$)[4] were prepared according to the literature procedures. Dichloromethane, toluene, and tetrahydrofuran were purified according to published procedures.[20] All of the compounds were characterized by melting points, IR, ^{1}H NMR, ^{13}C NMR, MS and elemental analysis.

Instrumentation

The ^{1}H NMR spectra were recorded in $CDCl_3$ on a General Electric QE-300 NMR spectrometer and the chemical shifts are reported in ppm units downfield from internal tetramethylsilane. Infrared spectra were recorded on a Nicolet 10 DX FT spectrometer. Gas chromatography was performed on a Hewlett-Packard 5890A gas chromatograph equipped with a HP 3392 integrator. GC-MS analyses were carried out on a Hewlett-Packard 5890 gas chromatograph interfaced to a HP 5970 mass spectrometer.

Synthesis

The synthesis of the polyphenylenes in Chart I was carried out via the coupling of 2,5-dimethoxy-4-methylphenylmagnesium bromide (or iodide) with the requisite aryl bromide in the presence of bis(triphenylphosphine)palladium(II) chloride as a catalyst.[21]

General procedure. A solution of 2,5-dimethoxy-4-methylmagnesium bromide was prepared from 4-bromo-2,5-dimethoxytoluene[16] (4.62 g, 20 mmol) and magnesium turnings (1.44 g, 60 mmol) in anhydrous tetrahydrofuran (30 mL) under an argon atmosphere. The Grignard reagent was transferred by a hypodermic syringe to a Schlenk flask containing a mixture of 1,4-dibromobenzene (2.12 g, 9 mmol) and a catalytic amount of bis(triphenylphosphine)palladium(II) chloride (50 mg, 0.08 mmol) in anhydrous tetrahydrofuran (20 mL) under an argon atmosphere. The pale yellow reaction mixture was refluxed for 10–70 h, and then poured into 200 mL of water. The aqueous phase layer was further extracted with dichloromethane (3 × 100 mL). The combined organic extracts were dried over anhydrous magnesium sulfate, and the solvent was removed in vacuo. The residue was purified by flash chromatography on silica gel with hexane, and then hexane–dichloromethane (3 : 1) as the eluents. The product was further recrystallized from ethanol to afford the desired polyphenylene **2** (3.0 g, 94%). The characteristic spectral data for the various polyphenylenes are given below.

4,4′-Dimethyl-2,2′,5,5′-tetramethoxy-1,1′-biphenyl 1. Mp 135 °C (lit.[22] 133 °C); yield: 96%; IR (cm^{-1}): 2973, 2367, 2338, 1865, 1787, 1460, 1230, 1211, 1072, 975, 926, 842, 757, 715, 703, 636, 612, 539, 412; ^{1}H NMR ($CDCl_3$): δ 6.82 (s, 2H), 6.78 (s, 2H), 3.79 (s, 6H), 3.74 (s, 6H), 2.27 (s, 6H); ^{13}C NMR ($CDCl_3$): δ 151.4, 150.6, 126.5, 125.3, 114.9, 113.8, 56.6, 56.0, 16.4; MS (m/z): 303 (M^+ + 1, 17%), 302 (M^+, 100), 287 (29) 272 (25), 257 (22), 256 (40).

4,4″-Dimethyl-2,2″,5,5″-tetramethoxy-1,1′:4′,1″-terphenyl 2. Mp 188 °C; yield: 94%; IR (cm^{-1}): 2943, 2827, 2367, 2337, 1538, 1501, 1465, 1393, 1211, 1047, 848, 799, 726, 624, 533, 460, 442, 412; ^{1}H NMR ($CDCl_3$): δ 7.58 (s, 4H), 6.88 (s, 2H), 6.83 (s, 2H), 3.83 (s, 6H), 3.78 (s, 6H), 2.17 (s, 6H); ^{13}C NMR ($CDCl_3$): δ 151.8, 150.2, 137.1, 129.1, 128.2, 126.5, 114.9, 113.2, 56.4, 56.0, 16.3; MS (m/z): 379 (M^+ + 1, 26%) 378 (M^+, 100), 363 (12), 349 (11), 348 (45), 333 (12); Anal. Calcd. for $C_{24}H_{26}O_4$: C, 76.19; H, 6.88. Found: C, 76.11; H, 6.91%.

4,4‴-Dimethyl-2,2‴,5,5‴-tetramethoxy-1,1′:4′,1″:4″,1‴-quaterphenyl 3. Mp 192 °C; yield: 73%; IR (cm^{-1}): 3001, 2924, 2840, 2362, 2341, 1497, 1462, 1391, 1216, 1047, 1005, 864, 850, 836, 822, 801, 674; ^{1}H NMR ($CDCl_3$): δ 7.63–7.72 (m, 8H), 6.90 (s, 2H), 6.86 (s, 2H), 3.86 (s, 6H) 3.80 (s, 6H), 2.30 (s, 6H); ^{13}C NMR($CDCl_3$): δ 151.9, 150.2, 139.5., 137.6, 129.8, 127.9, 126.8, 126.7, 114.9, 113.1, 56.4, 56.0, 16.3; MS (m/z): 455 (M^+ + 1, 34%), 454 (M^+, 100), 424 (23), 227 (12), 212 (15), 204 (12); Anal. Calcd. for $C_{30}H_{30}O_4$: C, 79.30; H, 6.61. Found: C, 79.35; H, 6.62%.

4,4⁗-Dimethyl-2,2⁗,5,5⁗-tetramethoxy-1,1′:4′,1″:4″,1‴:4‴,1⁗-quinquiphenyl 4. Mp 203 °C; yield: 46%; IR (cm^{-1}): 2930, 2840, 2367, 2331, 1495, 1477, 1393, 1217, 1047, 1005, 866, 848, 829, 805, 757, 708, 666, 533, 484, 430; ^{1}H NMR ($CDCl_3$): δ 7.55–7.74 (m, 12H), 6.90 (s, 2H), 6.86 (s, 2H), 3.86 (s, 6H),

3.80 (s, 6H), 2.30 (s, 6H); ^{13}C NMR ($CDCl_3$): δ 151.9, 150.2, 139.8, 139.1, 137.7, 129.8, 127.9, 127.4, 126.7, 126.6, 114.9, 113.1, 56.4, 56.1, 16.3; Anal. Calcd. for $C_{36}H_{34}O_4$: C, 81.51; H, 6.42. Found: C, 81.56; H, 6.42%.

4,4‴″-Dimethyl-2,2‴″,5,5‴″-tetramethoxy- 1,1′:4′,1″:4″,1‴:4‴,1‴″:4‴″,1‴″-sexiphenyl[23]5. Mp 228 °C; yield 85%; IR (cm^{-1}): 3027, 2997, 2943, 2918, 2840, 2827, 2373, 2349, 1489, 1471, 1393, 1277, 1211, 1047, 1005, 860, 817, 799, 733, 714, 660, 563, 508, 484, 460, 436; ^{1}H NMR ($CDCl_3$): δ 7.64–7.74 (m, 16H), 6.89 (s, 2H), 6.85 (s, 2H), 3.86 (s, 6H), 3.80 (s, 6H), 2.31 (s, 6H); ^{13}C NMR ($CDCl_3$): δ 151.9, 150.2, 150.0, 139.9, 139.5, 139.1, 137.8, 129.8, 127.9, 127.4, 127.3, 126.7, 115.0, 113.1, 56.4, 56.0, 16.3; Anal. Calcd. for $C_{42}H_{38}O_4$: C, 83.17; H, 6.27. Found: C, 82.71; H, 6.25%.

2′,4,4″-Trimethyl-2,2″,5,5″-tetramethoxy-1,1′:4′,1″:4″,1‴-terphenyl 6. Mp 190–191 °C; yield: 57%; ^{1}H NMR ($CDCl_3$): δ 7.43–6.83 (m, 7H), 3.86 (s, 3H), 3.82 (s, 6H), 3.76 (s, 3H), 2.32 (s, 3H), 2.31 (s, 3H), 2.43 (s, 3H); ^{13}C NMR ($CDCl_3$): δ 151.8, 151.5, 150.4, 150.2, 137.5, 137.3, 136.5, 130.6, 130.0, 128.5, 126.7, 126.2, 115.0, 114.8, 114.7, 114.2, 113.7, 113.4, 56.4, 56.2, 56.1, 56.0, 20.2, 16.4, 16.3; MS (m/z): 392 (M^+, 11%), 181 (14), 173 (10), 147 (22), 74 (9), 73 (100); Anal. Calcd. for $C_{25}H_{28}O_4$: C, 76.53; H, 7.14. Found: C, 75.97; H, 7.14%.

2′,4,4″,5′-Tetramethyl-2,2″,5,5″-tetramethoxy-1,1′:4′,1″:4″,1‴-terphenyl 7. Mp 196 °C; yield: 17%; IR (cm^{-1}): 2949, 2910, 2852, 2827, 2373, 2337, 1520, 1495, 1459, 1399, 1296, 1205, 1181, 1053, 1035, 860, 799, 769, 720, 484; ^{1}H NMR ($CDCl_3$): δ 7.43 (s, 2H), 6.96 (s, 2H), 6.91 (s, 2H), 3.97 (s, 6H), 3.92 (s, 6H), 2.47 (s, 6H), 2.32 (s, 6H); ^{13}C NMR ($CDCl_3$): δ 151.4, 150.2, 137.4, 133.8, 131.3, 128.4, 126.0, 113.9, 113.7, 56.1, 55.9, 19.5, 16.3; MS (m/z): 407 (M^+ + 1, 26%) 406 (M^+, 100), 376 (19); Anal. Calcd. for $C_{26}H_{30}O_4$: C, 76.85; H, 7.39. Found: C, 76.81; H, 7.43%.

2′,3′,4,4″,5′,6′-Hexamethyl-2,2″,5,5″-tetramethoxy-1,1′:4′,1″:4″,1‴-terphenyl 8. Yield 12%; the cis and trans isomers were separated by flash chromatography on silica gel with dichloromethane–hexane (1:9 v/v) and characterized separately: cis-isomer: mp 190 °C; IR (cm^{-1}): 2997, 2949, 2930, 2840, 2367, 2337, 1508, 1471, 1417, 1393, 1284, 1205, 1181, 1047, 1005, 878, 805, 755, 714, 690, 672, 490, 448; ^{1}H NMR ($CDCl_3$): δ 6.81 (s, 2H), 6.58 (s, 2H), 3.77 (s, 6H), 3.69 (s, 6H), 2.30 (s, 12H), 1.97 (s, 6H); ^{13}C NMR ($CDCl_3$): δ 151.6, 150.4, 137.4, 132.2, 129.1, 125.6, 114.6, 113.6, 56.3, 56.1, 17.9, 16.4; trans-isomer: mp 205 °C; IR (cm^{-1}): 2996, 2842, 2368, 1508, 1471, 1417, 1393, 1284, 1205, 1181, 1047, 1005, 878, 805, 755, 714, 690; ^{1}H NMR ($CDCl_3$): δ 6.82 (s, 2H), 6.62 (s, 2H), 3.78 (s, 6H), 3.74 (s, 6H), 2.31 (s, 12H), 1.97 (s, 6H); ^{13}C NMR ($CDCl_3$): δ 151.6, 150.4, 137.1, 132.0, 129.0, 125.4, 114.2, 113.7, 56.4, 56.0, 17.9, 16.4; cis–trans mixture MS (m/z): 435 (M^+ + 1, 27%) 434 (M^+, 100), 404 (13), 217 (13); Anal. Calcd. for $C_{28}H_{34}O_4$: C, 77.42; H, 7.83. Found: C, 77.71; H, 7.83%.

2,7-Bis(4′-methyl-2′,5′-dimethoxyphenyl)-9,9-dimethylfluorene, 9. Mp 213 °C; yield: 69%; IR (cm^{-1}): 3051, 2991, 2955, 2930, 2840, 2834, 2373, 2343, 1514, 1465, 1399, 1374, 1328, 1296, 1259, 1211, 1175, 1150, 1047, 1005, 878, 860, 821, 781, 745, 720, 678, 661, 496, 448; ^{1}H NMR ($CDCl_3$): δ 7.76 (d, J 7.8 Hz, 2H), 7.63 (s, 2H), 7.55 (d, J 7.8 Hz, 2H), 6.92 (s, 2H), 6.86 (s, 2H), 3.87 (s, 6H), 3.80 (s, 6H), 2.32 (s, 6H), 1.57 (s, 6H); ^{13}C NMR ($CDCl_3$): δ 153.6, 151.9, 150.1, 137.8, 137.4, 128.8, 128.2, 126.5, 123.7, 119.5, 115.1, 113.3, 56.5, 56.1, 46.9, 27.2, 16.3; MS (m/z): 495 (M^+ + 1, 39%) 494 (M^+, 100), 479 (15), 449 (12), 247, (19), 232 (20), 217 (17); Anal. Calcd. for $C_{33}H_{34}O_4$: C, 80.16; H, 6.88. Found: C, 80.13; H, 6.99%.

<u>trans</u>-4,4′-Bis(2′,5′-dimethoxy-4′-methylphenyl)stilbene 11. Mp 197 °C; yield: 30%; IR (cm^{-1}): 2990, 2828, 2366, 2332, 1521, 1492, 1465, 1393, 1374, 1211, 1046, 835, 702, 593; ^{1}H NMR ($CDCl_3$): δ 7.59 (s, 4H), 7.58 (s, 4H), 7.20 (s, 2H), 6.87 (s, 2H), 6.85 (s,2H), 3.86 (s, 6H), 3.79 (s, 6H), 2.32 (s, 6H); ^{13}C NMR ($CDCl_3$): δ 151.9, 150.2, 138.0, 136.0, 129.7, 128.3, 128.1, 126.8, 126.2, 115.2, 113.0, 56.5, 56.1, 16.3;

MS (m/z): 481 (M^+ + 1, 40%) 480 (M^+, 100), 240 (34), 239 (20), 233 (15), 225 (60), 218, (23); Anal. Calcd. for $C_{32}H_{32}O_4$: C, 80.00; H, 6.67. Found: C, 79.15; H, 6.89%.

1,2-Bis(2′,5′-dimethoxy-4′-methylbiphenyl-4-yl)acetylene 12. Mp 195 °C; yield: 52%; ^{1}H NMR ($CDCl_3$): δ 7.55–7.62 (m, 8H), 6.85 (s, 4H), 3.86 (s, 6H), 3.78 (s, 6H), 2.31 (s, 6H); ^{13}C NMR ($CDCl_3$): δ 152.1, 150.3, 138.7, 131.3, 129.4, 127.2, 122.0, 115.3, 113.0, 89.9, 56.5, 56.1, 16.3; MS (m/z): 479 (M^+ + 1, 35%) 478 (M^+, 100), 239 (20), 233 (15), 225 (60), 218 (23), 207 (40); Anal. Calcd. for $C_{32}H_{30}O_4$: C, 80.33; H, 6.28. Found: C, 81.05; H, 6.23%.

4,4′-Bis(2′,5′-dimethoxy-4′-methylphenyl)bibenzyl 10. According to the literature procedure,[24] a mixture of 100 mg (0.2 mmol) of **12** and 100 mL of ethyl acetate was placed in a standard Paar bottle along with 20 mg of 10% palladium on carbon catalyst and the mixture hydrogenated at an initial pressure of 60 psi. It was recrystallized from ethanol–dichloromethane to give 99 mg (98%) of **10** as a white solid: mp 196–197 °C; ^{1}H NMR ($CDCl_3$): δ 7.52 (d, J 7.8 Hz, 4H), 7.34 (d, J 8.1 Hz, 4H), 6.87 (s, 2H), 6.85 (s, 2H), 3.85 (s, 6H), 3.78 (s, 6H), 3.03 (s, 4H), 2.30 (s, 6H); ^{13}C NMR ($CDCl_3$): δ 151.9, 150.2, 140.5, 136.4, 129.5, 128.5, 128.1, 126.4, 115.1, 113.3, 56.5, 56.1, 37.7, 16.3; MS (m/z): 482 (M^+, 10%), 242 (16), 241 (100), 226 (9), 211 (24); Anal. Calcd. for $C_{32}H_{34}O_4$: C, 79.67; H, 7.05. Found: C, 79.59; H, 6.83%.

Bis(2′,5′-dimethoxy-4′-methylbiphenyl-4-yl) ether 13. Mp 197 °C; yield: 87%; ^{1}H NMR ($CDCl_3$): δ 7.53 (d, 4H, J 7.8 Hz), 7.11 (d, 4H, J 7.8 Hz), 6.83 (s, 4H), 3.84 (s, 6H), 3.77 (s, 6H), 2.39 (s, 6H); ^{13}C NMR ($CDCl_3$): δ 151.8, 150.1, 133.6, 130.7, 127.8, 126.5, 118.5, 115.0, 113.1, 56.4, 56.1, 16.3; MS (m/z): 471 (M^+ + 1, 35%) 470 (M^+, 100), 239 (20), 243 (48).

Cyclic voltammetry

Cyclic voltammetry (CV) was performed on a BAS 100A Electrochemical Analyzer with a cell of airtight design with high vacuum Teflon valves and Viton O-ring seals to allow an inert atmosphere to be maintained without contamination by grease. The working electrode consisted of an adjustable platinum disk embedded in a glass seal to allow periodic polishing (with a fine emery cloth) without significantly changing the surface area (~1 mm^2). The saturated calomel electrode (SCE) and its salt bridge were separated from the cathode by a sintered glass frit. The counter electrode consisted of a platinum gauze that was separated from the working electrode by ~3 mm. The measurements were carried out in a solution of 0.1 M supporting electrolyte (tetra-n-butylammonium hexafluorophosphate) and 5 × 10^{-4} M compound in dry dichloromethane under an argon atmosphere. All cyclic voltammograms were measured at the same sweep rate of 2 V s^{-1} with iR compensation. The potentials were referenced to SCE which was calibrated with added ferrocene (5 × 10^{-4} M). Controlled-potential coulometry was conducted with an EG&G Princeton Applied Research (PAR) 173 potentiostat and digital coulometer. The number of electrons transferred was calculated from the relation n = Q/Fm, where F is the Faraday constant, m is the moles of the material, and Q is the coulomb reading at the time the current dropped to <3–9% of its original value. The oxidation potentials E_{ox} are listed in Table 1.

Chemical oxidation via electron exchange with aromatic cation radicals

A 1 cm quartz cuvette equipped with a Schlenk adaptor was charged with a freshly prepared solution of a donor with $OMN^{+\bullet}$ $SbCl_6^-$ (E^0_{red} = 1.34 V vs. SCE[15,20]) generated in situ in anhydrous dichloromethane from the neutral OMN and $NOSbCl_6$. The solution immediately took on a greenish yellow coloration and the UV-Vis-NIR absorption spectrum was recorded in a Cary UV-Vis-NIR Spectrometer.

Diffuse-reflectance spectroscopy

The crystals of cation–radical hexachloroantimonate salts were mixed with potassium hexafluorophosphate (KPF_6) and ground to a fine powder to form a 20 wt% dispersion, and stored in a 1 mm quartz cuvette. The diffuse-reflectance spectra were collected in a Cary 500 UV-Vis-NIR Spectrometer. The spectra were presented as percentage absorption (%ABS) as defined by $\%ABS = 100(1 - R/R_0)$ with R and R_0 representing the intensities of the diffuse-reflected probe light and of the reference light, respectively.

General procedure for X-ray crystallography of the cation–radicals

A greenish yellow solution of triethyloxonium hexachloroantimonate (Et_3O^+ $SbCl_6^-$) (1.5 mM) and **1** (1 mM) in dichloromethane (20 mL) was prepared under an argon atmosphere at room temperature.[25] The solution was carefully layered with toluene and refrigerated (−20 °C) to afford dark green single crystals as of the cation–radical salt ($\mathbf{1}^{+\cdot}\cdot SbCl_6^-$) suitable for the X-ray crystallographic analysis. Single crystals of other cation–radical salts ($B^{+\cdot+\cdot}\cdot 2SbCl_6^-$, $\mathbf{2}^{+\cdot}\cdot SbCl_6^-$, $\mathbf{3}^{+\cdot}\cdot SbCl_6^-$, and $\mathbf{9}^{+\cdot}\cdot SbCl_6^-$) were isolated using the same procedure. Single crystals of the neutral donors, **A**, **B**, **1**, **2** and **8** were obtained by slow evaporation of the solvent. The intensity data were collected with the aid of a Siemens SMART diffractometer equipped with a CCD detector using Mo-Kα radiation (λ = 0.71073 Å), at −150 °C unless otherwise specified. The structures were solved by direct methods[26] and refined by a full matrix least-squares procedure with IBM Pentium and SGI O_2 computers.‡

Crystal Data. Donor **A**. $C_{10}H_{14}O_2$, M = 166.21, monoclinic, space group $P2_1/n$, a = 6.4943(4), b = 8.9209(5), c = 8.0240(5) Å, β = 101.82(1)°, U = 455.02(5) Å^3, Z = 2, D_x = 1.213 g cm^{-3}, μ = 0.083 mm^{-1}, 4073 reflections (1987 unique) with 2θ ≤ 72.5°, 57 variables refined to R = 0.049 [1593 observed data, I ≥ 2σ(I)], wR(F^2) = 0.120, $\Delta\rho_{min}/\Delta\rho_{max}$ = −0.25/0.53 e Å^{-3}. Donor **B**. $C_{21}H_{28}O_4$, M = 344.43, T = 93(2) K, orthorhombic, space group $P2_12_12_1$, a = 7.8130(5), b = 7.9994(5), c = 29.763(2) Å, U = 1860.2(2) Å^3. Z = 4, D_x = 1.230 g cm^{-3}, μ = 0.084 mm^{-1}, 23294 reflections (4699 unique) with 2θ ≤ 71.8°, 338 variables refined to R = 0.039 [4102 observed data, I ≥ 2σ(I)], wR(F^2) = 0.094, $\Delta\rho_{min}/\Delta\rho_{max}$ = −0.19/0.40 e Å^{-3}. Compound $\mathbf{B}^{+\cdot+\cdot}$. $C_{21}H_{28}O_4^{++}$ $2SbCl_6^-$, M = 1013.33, monoclinic, space group $P2_1/m$, a = 8.073(2), b = 26.577(5), c = 8.445(2) Å, β = 98.99(3)°, U = 1789.6(6) Å^3. Z = 2, D_x = 1.881 g cm^{-3}, μ = 2.432 mm^{-1}, 22003 reflections (8082 unique) with 2θ ≤ 72.1°, 190 variables refined to R = 0.047 [5945 observed data, I ≥ 2σ(I)], wR(F^2) = 0.093, $\Delta\rho_{min}/\Delta\rho_{max}$ = −2.19/1.37 e Å^{-3}. Donor **1**. $C_{18}H_{22}O_4$, M = 302.36, monoclinic, space group C2/c, a = 22.199(1), b = 5.8270(3), c = 12.6965(7) Å, β = 109.85(1)°, U = 1544.8(1) Å^3. Z = 4, D_x = 1.300 g cm^{-3}, μ = 0.091 mm^{-1}, 10207 reflections (3439 unique) with 2θ ≤ 72.2°, 103 variables refined to R = 0.058 [1847 observed data, I ≥ 2σ(I)], wR(F^2) = 0.137, $\Delta\rho_{min}/\Delta\rho_{max}$ = −0.25/0.39 e Å^{-3}. Compound $\mathbf{1}^{+\cdot}$. $C_{18}H_{22}O_4^+$ $SbCl_6^-$, M = 636.81, triclinic, space group $P\bar{1}$, a = 7.6596(2), b = 12.8575(3), c = 13.7700(3) Å, α = 62.369(1), β = 83.190(1), γ = 83.567(1)°, U = 1190.47(5) Å^3. Z = 2, D_x = 1.777 g cm^{-3}, μ = 1.855 mm^{-1}, 17125 reflections (10303 unique) with 2θ ≤ 72.2°, 271 variables refined to R = 0.045 [7229 observed data, I ≥ 2σ(I)], wR(F^2) = 0.070, $\Delta\rho_{min}/\Delta\rho_{max}$ = −0.99/0.82 e Å^{-3}. Donor **2**. $C_{24}H_{26}O_4$, M = 378.45, triclinic, space group $P\bar{1}$, a = 5.0760(3), b = 13.9623(9), c = 14.3411(9) Å, α = 77.796(2), β = 88.587(2), γ = 88.641(2)°, U = 992.9(1) Å^3. Z = 2, D_x = 1.266 g cm^{-3}, μ = 0.085 mm^{-1}, 10726 reflections (5993 unique) with 2θ ≤ 62°, 295 variables refined to R = 0.099 [2535 observed data, I ≥ 2σ(I)], wR(F^2) = 0.233, $\Delta\rho_{min}/\Delta\rho_{max}$ = −0.46/0.60 e Å^{-3}. Compound $\mathbf{2}^{+\cdot}$. $C_{24}H_{26}O_4^+$ $SbCl_6^-$, M = 712.90, monoclinic, space group $P2_1/c$, a = 13.4765(2), b = 15.5512(3), c = 13.8393(3) Å, β = 105.944(1)°, U = 2788.8(1) Å^3. Z = 4, D_x = 1.698 g cm^{-3}, μ = 1.594 mm^{-1}, 34861 reflections (12599 unique) with 2θ ≤ 72.5°, 322 variables refined to R = 0.037 [9054 observed data, I ≥ 2σ(I)], wR(F^2) = 0.071, $\Delta\rho_{min}/\Delta\rho_{max}$ = − 1.48/0.70 e Å^{-3}. Compound $\mathbf{3}^{+\cdot}$. $C_{30}H_{30}O_4^+$ $SbCl_6^-$, M = 788.99, monoclinic, space group $P2_1$, a = 7.2182(1), b = 16.6646(3),

c = 13.4314(1) Å, β = 103.884(1)°, U = 1568.44(4) Å^3, Z = 2, D_x = 1.671 g cm^{-3}, μ = 1.426 mm^{-1}, 23274 reflections (13253 unique) with 2θ ≤ 71.3°, 376 variables refined to R = 0.046 [9677 observed data, I ≥ 2σ(I)], wR(F^2) = 0.067, $\Delta\rho_{min}/\Delta\rho_{max}$ = −0.70/0.90 e Å^{-3}. Donor **8**. $C_{28}H_{34}O_4$, M = 434.55, T = 93 (2) K, monoclinic, space group C2/c, a = 22.028(1), b = 7.3676(3), c = 14.2868(6) Å, β = 94.883(1)°, U = 2310.2(5) Å^3. Z = 4, D_x = 1.249 g cm^{-3}, μ = 0.082 mm^{-1}, 16277 reflections (5036 unique) with 2θ ≤ 71.2°, 225 variables refined to R = 0.040 [3995 observed data, I ≥ 2σ(I)], wR(F^2) = 0.116, $\Delta\rho_{min}/\Delta\rho_{max}$ = − 0.23/0.55 e Å^{-3}. Compound $\mathbf{9}^{+\cdot}$. $C_{33}H_{34}O_4^{+}$ $SbCl_6^{-}\cdot 1.76(CH_2Cl_2)$, M = 978.95, triclinic, space group $P\bar{1}$, a = 13.1454(2), b = 13.4568(3), c = 14.1244(3) Å, α = 103.375(1), β = 101.858(1), γ = 116.056(1)°, U = 2044.97(5) Å^3. Z = 2, D_x = 1.590 g cm^{-3}, μ = 1.334 mm^{-1}, 32329 reflections (16881 unique) with 2θ ≤ 71.2°, 491 variables refined to R = 0.043 [11957 observed data, I ≥ 2σ(I)], wR(F^2) = 0.089, $\Delta\rho_{min}/\Delta\rho_{max}$ = −1.51/1.61 e Å^{-3}.

Acknowledgements

We thank the R. A. Welch Foundation and the National Science Foundation for financial support. We also thank Dr P. Le Maguères for the X- ray analyses of **B** and $\mathbf{B}^{+\cdot+\cdot}$.

References

1. (*a*) J. M. Tour, *Acc. Chem. Res.,* 2000, 33, 791; (*b*) J. Roncali, *Acc. Chem. Res*., 2000, 33, 147; (*c*) F. Barigelletti and L. Flamigni, *Chem. Soc. Rev*., 2000, 29, 1; (*d*) W. B. Davis, W. A. Svec, M. A. Ratner and M. R. Wasielewski, *Nature*, 1998, 396, 60; (*e*) L. A. Bumm, J. J. Arnold, M. T. Cygan, T. D. Dunbar, T. P. Burgin, L. Jones, II, D. L. Allara, J. M. Tour and P. S. Weiss, *Science*, 1996, 271, 1705; (*f*) A. P. deSilva Ed., Molecular-level Electronics. In: *Electron Transfer in Chemistry*, V. Balzani, Ed., vol. 5, Wiley, New York, 2001.
2. (*a*) A. S. Lukas, P. J. Bushard and M. R. Wasielewski, *J. Am. Chem. Soc*., 2001, 123, 2440; (*b*) S. Fraysse, C. Coudret and J.-P. Launay, Eur. *J. Inorg. Chem*., 2000, 1581; (*c*) C. P. Collier, G. Mattersteig, E. W. Wong, Y. Luo, K. Beverly, J. Sampaio, F. M. Raymo, J. F. Stoddart and J. R. Heath, *Science*, 2000, 289, 1172; (*d*) A. P. de Silva, H. Q. N. Gunaratne, T. Gunnlaugsson, A. J. M. Huxley, C. P. McCoy, J. T. Rademacher and T. E. Rice, *Chem. Rev*., 1997, 97, 1515.
3. (*a*) R. M. Metzger, Acc. Chem. Res., 1999, 32, 950; (*b*) J. Chen, M. A. Reed, A. M. Rawlett and J. M. Tour, *Science*, 1999, 286, 1550.
4. R. Rathore, A. S. Kumar, S. V. Lindeman and J. K. Kochi, *J. Org. Chem*., 1998, 63, 5847.
5. (*a*) B. Badger and B. Brocklehurst, *Trans, Faraday Soc*., 1969, 65, 2582 and 2588 RSC ; (*b*) B. Badger and B. Brocklehurst, *Trans, Faraday Soc*., 1970, 66, 2939; (*c*) J. K. Kochi, R. Rathore and P. Le Maguéres, *J. Org. Chem*., 2000, 65, 6826.
6. (*a*) D. K. Kyriacou, *Modern Electroorganic Chemistry*, Springer, Berlin, 1994; (*b*) A. J. Fry, *Synthetic Organic Electrochemistry*, Wiley, New York, 1989.
7. F. H. Allen, O. Kennard, D. G. Watson, L. Brammer, A. G. Orpen and R. Taylor, *J. Chem. Soc*., *Perkin Trans*. 2, 1987, S1.
8. R. Rathore, S. V. Lindeman, A. S. Kumar and J. K. Kochi, *J. Am. Chem. Soc*, 1998, 120, 6931.
9. P. Le Maguères, S. V. Lindeman and J. K. Kochi, *Organometallics*, 2001, 20, 115.
10. P. Le Maguères, S. V. Lindeman and J. K. Kochi, *J. Chem. Soc*.,Perkin Trans. 2, 2001, 1180.
11. Although the cation–radical of **A** was stable in solution (as established by the reversible CV), it was not sufficiently persistent to allow isolation of the cation–radical salt $\mathbf{A}^{+\cdot}$ $SbCl_6^{-}$. Thus $\mathbf{B}^{+\cdot+\cdot}$

and not $\mathbf{A}^{+\cdot}$ was used to establish the geometrical (bond-length) change in D upon 1-electron oxidation to the cation–radical $\mathbf{D}^{+\cdot}$ with q = 1.
12. All the aromatic donors in Classes I–III show chemically reversible cyclic voltammograms with anodic/cathodic peak current ratio in the value: $0.9 < i_p^a/i_p^c < 1.1$. The quantitative electrode behavior relative to the electrochemical reversibility of these interesting redox couples will be addressed in a later study.
13. (*a*) Such a stabilization energy may be described in quantum mechanical terms, as the electronic coupling element H_{AB}. See, e.g. C. Creutz, M. D. Newton and N. Sutin, *J. Photochem. Photobiol. A: Chem*., 1994, 82, 47; (*b*) The comproportionation constants (and hence the free energy changes) between cation–radicals and their dications will be presented separately.
14. (*a*) L. Pauling, *Nature of the Chemical Bond*, Cornell University Press, Ithaca, New York, 1960, p. 280; (*b*) S. M. Hubig, S. V. Lindeman and J. K. Kochi, *Coord. Chem. Rev*., 2000, 200–202, 831.
15. G. S Hiers and F. D. Hager, *Org. Synth*., 1932, Coll. Vol. I, 58.
16. D. McHale, P. Mamalis, J. Green and S. Marcinkiewicz, *J. Chem. Soc*., 1958, 1600.
17. H. France, I. M. Heilbron and D. H. Hey, *J. Chem. Soc*., 1938, 1364.
18. R. G. Harvey, P. P. Fu and P. W. Rabideau, *J. Org. Chem*., 1976, 41, 2706.
19. (*a*) R. N. McDonald and T. W. Campbell, in *Organic Syntheses*, Wiley, New York, 1973, vol. 5, p. 499; (*b*) S. Misumi, M. Kuwana and M. Nakagawa, *Bull. Chem. Soc. Jpn*., 1962, 35, 135; (*c*) R. E. Moser and H. G. Cassidy, *J. Org. Chem*., 1965, 30, 2602; (*d*) R. Rathore, E. Bosch and J. K. Kochi, Tetrahedron, 1994, 50, 6727.
20. D. D. Perrin, W. L. F. Armarego and D. R. Perrin, *Purification of Laboratory Chemicals*, 2nd edn., Pergamon, New York, 1980.
21. K. Kumada, *Pure Appl. Chem*., 1980, 52, 669 and references therein.
22. T. Jempty, K. A. Z. Gogins, Y. Mazur and L. Miller, *J. Org. Chem*., 1981, 46, 4545.
23. **5** was prepared by the coupling between 2,5-dimethoxy-4-methyl-4″-bromo-1,1′:4′,1″-terphenyl and its Grignard derivative.
24. P. G. Gassman and K. T. Mansfield, *Org. Synth*., 1973, Coll. Vol. V, 96.
25. Note that the UV-Vis-NIR absorption of various polyphenylene cation–radicals generated by triethyloxonium hexachloroantimonate (Et_3O^+ $SbCl_6$) were identical in all respect to those generated by $\mathbf{OMN}^{+\cdot}$ $SbCl_6$ in anhydrous dichloromethane.
26. G. M. Sheldrick, SHELXS-86, *Program for Structure Solution*, University of Göttingen, Germany, 1986.

Footnotes

† Dedicated in memoriam to Lennart Eberson, friend to whom oxidation mechanisms were a constant challenge.

‡ CCDC reference number(s) 162395–162404. See http://www.rsc.org/suppdata/p2/b1/b103139m/ for crystalographic files in .cif or other electronic format.